

Optimization of the characteristics of a relativistic electron beam based on laser wake-field acceleration using a non-symmetric gas target profile

D. Mancelli,^{1,2, a)} G. Andrianaki,^{1,2,3} I. Tazes,^{1,2} C. Vlachos,^{1,2,4} I. Fitis,^{1,2} I. Nikolos,³ M. Bakarezos,^{1,5} E. P. Benis,^{1,6} V. Dimitriou,^{1,5} N. A. Papadogiannis,^{1,5} and M. Tatarakis^{1,2}

¹⁾*Institute of Plasma Physics & Lasers, University Research & Innovation Centre, Hellenic Mediterranean University, 74100 Rethymno, Crete, Greece*

²⁾*Department of Electronic Engineering, School of Engineering, Hellenic Mediterranean University, 73133 Chania, Crete, Greece*

³⁾*School of Production Engineering & Management, Technical University of Crete, 73100 Chania, Greece*

⁴⁾*University of Bordeaux-CNRS-CEA, Centre Lasers Intenses et Applications, UMR 5107, 33405 Talence, France*

⁵⁾*Physical Acoustics and Optoacoustics Laboratory, Department of Music Technology & Acoustics, Hellenic Mediterranean University, 74100 Rethymnon, Greece*

⁶⁾*Department of Physics, University of Ioannina, 45110 Ioannina, Greece*

(Dated: 23 December 2025)

We demonstrate a high-energy, high-charge, electron source produced by the irradiation of a novel gaseous target by an ultra-intense femtosecond laser pulse. By exploiting a nonsymmetrical nozzle, we increased the total charge of the electron beam by at least an order of magnitude with respect to our previous experiments using symmetrical nozzles. In addition, the maximum energy of the accelerated electrons was enhanced by a factor of two. The electrons are accelerated via the Laser Wake-Field Acceleration mechanism. Particle-in-cell simulations indicate that electrons are injected via the ionization and the downramp injection mechanisms. Our measurements indicate that the demonstrated electron source is a considerable candidate for high dose, Very High Energy Electrons applications, such as radiotherapy.

I. INTRODUCTION

Particle acceleration is a research field that has been developing continuously for more than a century. The scientific and practical interest in charged particles and photon beams is wide; thus, huge investments have pushed the limits of accelerators' capabilities and potential. However, conventional accelerators are progressing by creating larger facilities, where longer acceleration length is allowed, increasing their size and consequent cost in values that are under criticism¹.

Laser technology has developed rapidly and, together with plasma science, provides an alternative, as Laser Plasma Accelerators (LPA) have achieved acceleration of high-energy particle beams in millimeter to centimeter distances by creating accelerating fields exceeding several orders of magnitude larger than those created by radiofrequency cavities. LPA are extensively studied either as standalone accelerators², or in combination with a previously accelerated beam injected in a Laser Wake-Field for a second acceleration stage³. Their reduction in size and cost is their main advantage, while the most important drawback is their stability/reproducibility⁴. As the accelerator is practically recreated per shot, the resulting beams present fluctuating characteristics (e.g. energy, energy spread, total charge, and pointing), which limit their potential applications. In addition, Laser Wake-

Field Acceleration (LWFA)⁵⁻⁷ is a method that simultaneously provides an electron and X-ray source, as oscillating electrons emit coherent betatron-type radiation in the keV range⁸⁻¹⁰. TerraWatt (TW) and PetaWatt (PW) lasers, hosted in university-scale facilities, are currently working to improve beam characteristics and gain control and reproducibility¹¹.

LWFA accelerates relativistic beams with pC¹² to nC¹³ total charge and energy up to a few GeV^{2,14}. LWFA occurs when a high-intensity, ultra-short laser pulse propagates through an under-dense, gaseous target profile^{15,16}. The pulse drives plasma waves along its propagation through the homogeneous ionized gas. Typically, in a high-intensity laser, the intensity of its pre-pulse already exceeds the ionization threshold of electrons of a hydrogen or helium gas; thus, after the pre-pulse propagation, the gas has already evolved into a plasma. The ponderomotive force of the main part of the laser pulse pushes electrons away from the area where the electric field is maximum, namely along the propagation axis, creating an ion bubble that matches the dimensions of the local laser beam size, which changes rapidly due to self-focusing and self-steepening effects. The electrons oscillate under the influence of the space charge force and form plasma waves, with an electron density-dependent plasma wavelength $\lambda_p[\mu m] = 33 \times (n_e[10^{18} cm^{-3}])^{-1/2}$, which follow the laser pulse up to its gradual vanishment. Under specific conditions, the wave amplitude increases and breaks at the rear side of the bubble, allowing the injection of energetic electrons into the bubble. This electron injection mechanism, known as self-injection¹⁷, is mainly responsible for the creation of low-energy-spread

^{a)} Authors to whom correspondence should be addressed; Electronic mail: dmancelli@hmu.gr

electron bunches. However, other injection mechanisms may occur, such as ionization injection, where a multi-electron gas is employed, either stand-alone or in a mixture with hydrogen or helium. In this case, the inner electrons of the multi-electron gas hold an ionization threshold exceeded only by the peak of the main part of the laser pulse or even by the laser intensity reached when self-focused. These electrons are ionized into the bubble and gain energy, resulting in a more populated bunch with high energy and high-energy spread^{9,18–20}. Another injection mechanism is the Downramp injection, which occurs when the laser pulse propagates along a density drop, commonly referred to as a downramp or density transition^{21–26}. The ion bubble along the density drop is longitudinally elongated, permitting the injection of lower-energy electrons at its rear side. Finally, acceleration of the injected electrons takes place along the laser propagation direction, following an inverse plasma density law. Acceleration is limited by several reasons, such as laser pulse diffraction or depletion. The length over which these are happening, affected by self-guiding effects, is a few mm for a TW laser and extends up to few cm for PW lasers. Another limitation is dephasing, where electrons enter the deceleration phase of the field and lose energy, a tunable limit as it is related to plasma density.

In TW facilities, the basic setup for LWFA consists of the optics for focusing the laser pulse down to a few micron-radius focal spots on a gas jet emanating from a pulsed gas valve. More sophisticated setups involving gas cells/capillaries are usually employed in PW lasers, where the laser pulse is depleted and diffracted over longer distances. In addition, when the downramp mechanism is studied, the gas flow is tailored via several techniques. When the scale length of the density drop is sharp, namely comparable to the plasma wavelength, often referred to as shock front injection, the density profile is achieved primarily by the use of a blade that partially interrupts the gas jet, resulting in the development of a shock, which is a short and abrupt increase in the density of the flow density^{26–29}. Another setup related to downramp injection is by optically shaping the plasma density, pre-forming a lower density channel where injection is provoked²⁴. On the other hand, a longer density drop is created mainly by implementing consecutive nozzles that produce an intersecting gas area of higher density, followed by a lower density area^{25,30,31}. The aforementioned setups provide some tunability over electron beam characteristics via controlling blade or nozzle positions, or nozzle backing pressure separately, and enhance reproducibility²⁵. However, complex and expensive equipment (e.g., translation stages and/or extra gas valves) is required³¹. In addition, due to the small size of the interaction area, the additional equipment is hard to establish in some configurations.

In this context, a novel idea is the use of a single non-symmetrical nozzle to create a downramp profile, which, to the best of our knowledge, has been so far re-

alized by only one group³². Our research team at the Institute of Plasma Physics and Lasers (IPPL) of the University Research & Innovation Centre of the Hellenic Mediterranean University (HMU) has performed systematic studies on electron acceleration using the LWFA method^{9,33–36}. In this work, we focus on the enhancement of the electron beam total charge with a goal of achieving a high-dose source. A high-dose source is preferable for use in biomedical applications and to generate efficient betatron radiation^{37,38}. The gaseous target is formed using, for the first time in our LWFA experiments, a novel in-house 3D-printed, non-symmetrical (NS) nozzle, designed to generate a unique gaseous density profile. The profile consists of a density downramp, followed by a quasi-constant density region aiming to enhance the downramp injection mechanism. The design of this nozzle removes the need for extra targetry features, thus reducing the setup complexity and making it favourable for applications. Following our previous work, we used the 45 TW Ti:Sa Zeus laser system for the irradiation of N₂ density profiles, thus combining several injection mechanisms, with the aim of maximizing the electron dose.

II. RESULTS AND DISCUSSION

The LWFA experimental setup layout is shown in Fig. 1^{33,39}. The main beam of the 45 TW Zeus laser system with a central wavelength at 807 nm, is focused 300 μm downstream of the exit of the nozzle. The focal spot of 28 μm diameter at Full Width Half Maximum (FWHM) is obtained using a 1.008 m focal length gold-coated off-axis parabola. The duration of the laser pulse is 24 fs, resulting in a mean intensity of the order of 10^{19} W/cm^2 ($a_0 \sim 2.5$). The NS nozzle is attached to an electromagnetic pulsed gas valve, triggered by the laser system to deliver the gas at tunable backing pressure. After the interaction, the accelerated electrons travelling in the laser propagation direction enter the magnetic spectrometer, which consists of two parallel magnetic plates with a magnetic field of 0.3 T and a scintillating screen (Lanex Regular). Electrons are deflected according to their energy due to the magnetic field, and after crossing the screen, the light emitted is collected by a calibrated optical system (lens and CCD camera)⁴⁰. The electron energy spectrum is calculated based on a home-developed algorithm⁴⁰. The secondary 10 mJ energy beam of Zeus laser system at the same laser wavelength and pulse duration is used as a probe beam for shadowgraphy measurements of the interaction.

The longitudinal length of the NS nozzle used in our experiments is 3.5 mm and was manufactured via 3D printing^{41–43}. The nozzle was printed via stereolithography, using an ANYCUBIC printer with a resolution of 0.05 mm on xy plane and 0.01 mm along z-axis. Fig. 2(a) presents a cross-section of the nozzle CAD design, along with a qualitative density distribution of the gas flow.

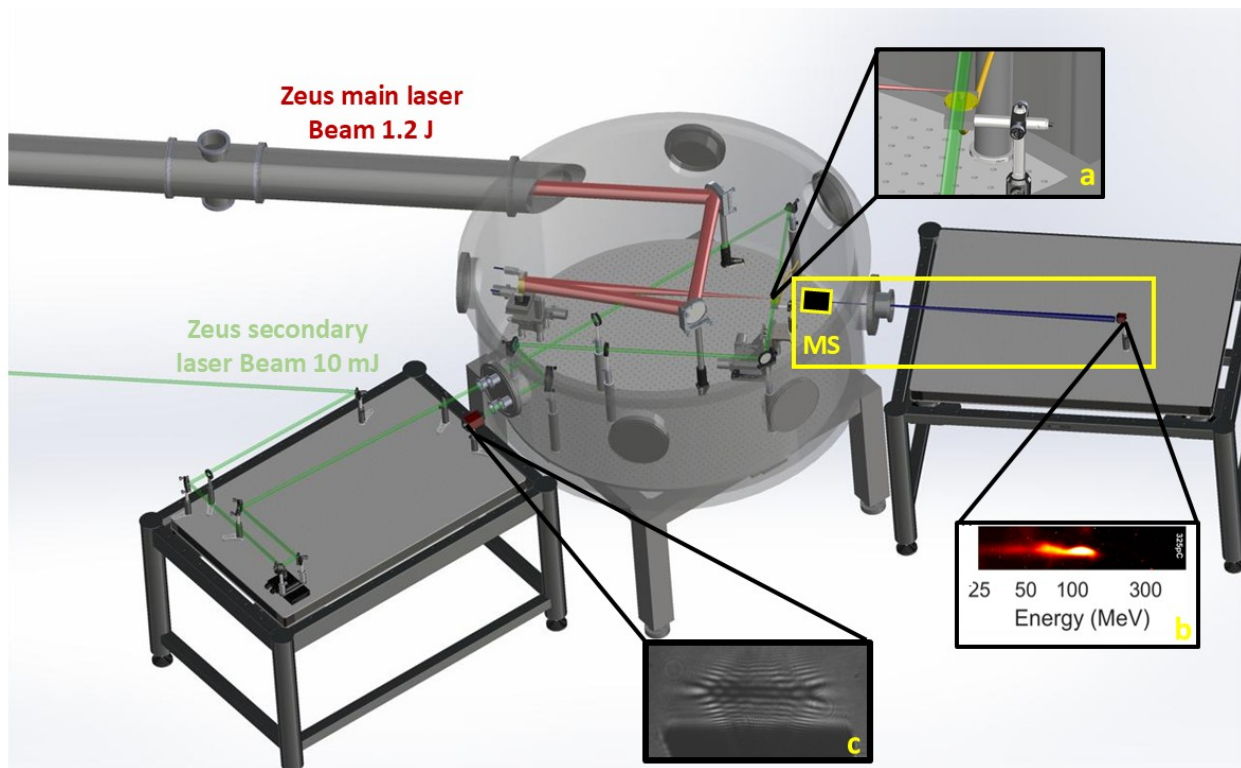


FIG. 1: The experimental setup. The main beam of the Zeus laser focuses downstream of the NS nozzle exit (a) and interacts with the gas. The accelerated electrons travelling in the laser propagation direction enter the magnetic spectrometer (MS), and their resulting spectra are recorded by a CCD (b). The low-energy, secondary beam serves to probe the interaction via shadowgraphy (c).

The throat is circular, with a diameter of $800\ \mu\text{m}$, in accordance with the specifications of the gas valve at the connecting region. Toward the exit, it is mainly extended in one direction, forming an asymmetric ellipse, whereas the opposite side is flat. The Mach number corresponding to the elliptical part of the nozzle is $M = 5.5$ deduced from Computational Fluid Dynamic simulations. Fig. 2(b) presents a section view of the N_2 density $300\ \mu\text{m}$ downstream the nozzle exit obtained using tomographic reconstruction^{44,45} of multiple interferograms (for more details on the method applied see^{43,46}). Fig. 2(c) shows the density line-out obtained along the dashed black line shown in Fig. 2(b), which coincides with the laser propagation axis. A high-density area is formed, with a peak $\sim 10^{18}$ particles/ cm^3 , which drops along a downward ramp within approximately $500\ \mu\text{m}$ length. For longer distances, an almost constant, lower-density area is evident.

The interaction of the laser with the gaseous profile resulted in the generation of electron bunches with beam-like characteristics. The variation of the electron beam characteristics was examined by changing the backing pressure applied at the gas valve inlet. In Fig. 3 characteristic shots are presented per backing pressure. The lower detection limit of the magnetic spectrometer was $25\ \text{MeV}$. At the low-pressure regime, high-charge, low-

energy electrons are seen to have a large divergence, measured with remarkable reproducibility at $\sim 20\ \text{mrad}$. By increasing backing pressure, the accelerated electrons improve their beam-like characteristics, having a lower divergence, while the electron energy increases and the total beam charge remains almost constant. The maximum energy is observed at a backing pressure of $45\ \text{bar}$ with the measured electron energy reaching $(300 \pm 20)\ \text{MeV}$, and divergence less than $10\ \text{mrad}$. An enhancement of the electron energy by at least a factor of two is achieved in comparison to our previous work. In addition, we would like to stress that the charge/dE/shot was enhanced by at least a factor of ~ 20 reaching a value of $0.2\ (\text{pC}/\text{pixel})$ instead of $0.01\ \text{pC}/\text{pixel}$ ³⁵, for N_2 gas, compared to our previous works where symmetrical nozzles were studied^{33,35,43}. The electron signal was observed in every shot, although variations in the energy spectra were evident as shown in Fig. 3. Thus, injection was ensured, and is attributed to the simultaneous occurrence of two injection mechanisms, downramp and ionization injection that take place during the interaction, as strongly suggested by Particle-In-Cell (PIC) simulations, presented below.

Fig. 4(a) shows the median total charge, in red-filled circles, with the statistical error bars for several shots, as a function of gas valve backing pressure. The total

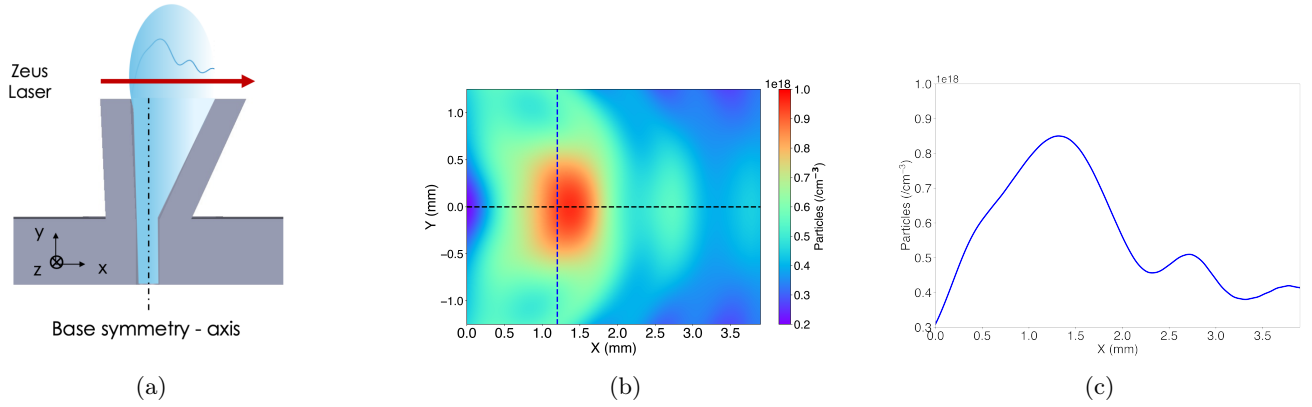


FIG. 2: (a) A CAD section view of the NS nozzle with a graph at the top indicating the produced gas density profile (blue line), along the laser propagation direction. (b) Plane view of the particle density 300 μm downstream the NS nozzle exit, obtained using a tomographic reconstruction method^{44,45}. (c) The density profile corresponding to the black dashed line of (b), namely the laser propagation axis at ($Y=0\text{ mm}$).

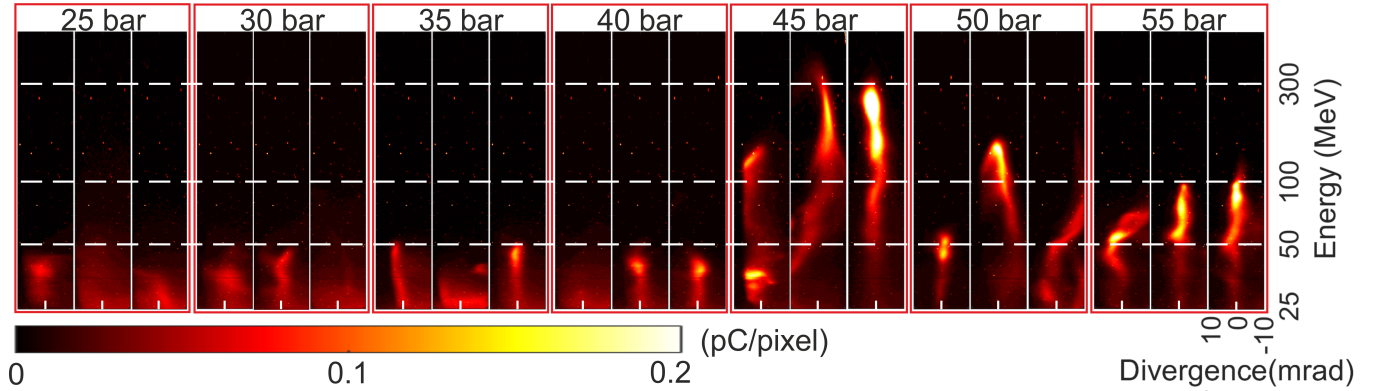


FIG. 3: A series of typical electron spectra measurements for different backing pressures at the gas valve inlet, ranging from 25 to 55 bar. Three representative shots per backing pressure are presented. The low energy limit of the spectrometer is 25 MeV. The charge per pixel corresponds to the colour bar, and the angular divergences are displayed.

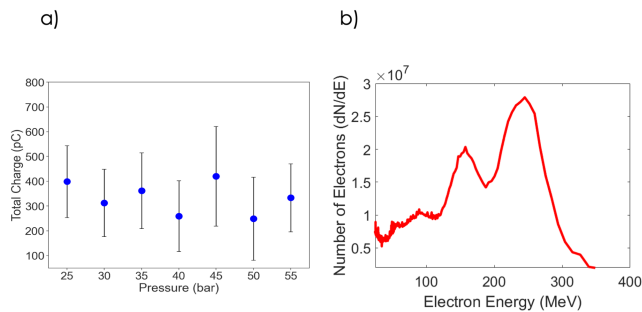


FIG. 4: (a) Total charge as a function of gas valve backing pressure. Measurements from 17-22 shots per backing pressure were averaged. (b) Energy spectrum of the highest energy shot at 45 bar backing pressure.

charge of each shot is found by integration of the signal over the whole area displayed on the CCD camera. The total charge remains almost constant with respect to the backing pressure.

Fig. 4(b) shows the electron energy spectrum for the case of the highest energy and total charge obtained at the optimum operating backing pressure window, found to be between 45 and 55 bar.

At all backing pressures there is a faint background (as, for instance is clearly shown in Fig. 3 at the low-energy area of the spectrum) which in some shots is present along the whole detector area. As evident in Fig. 3, by increasing the backing pressure, this faint background is drastically reduced, and the accelerated electron bunches acquire sharper beamlike characteristics. Within the optimum operating backing pressure window, the accelerator yields high energy, high-dose electron bunches with satisfying stability. The low-energy electron beams produced in the low-pressure regime are also useful, with the high

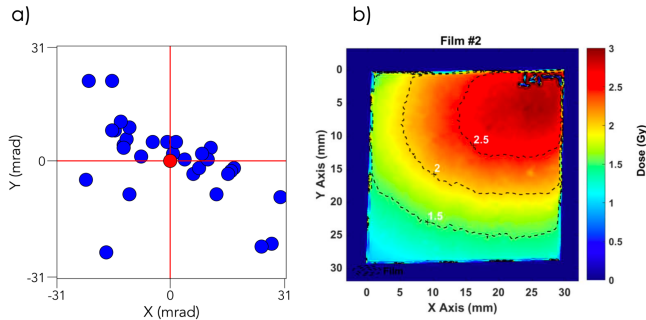


FIG. 5: (a) The beam pointing angle spread of the electron source (blue marks) of several consecutive shots. Red mark indicates the expected zero point and (b) 2D colour map of the measured absolute dose on the RCF Film aggregated over 140 shots. A clear iso-dose distribution ranging from 1.5 Gy the outer line to 2.5 Gy the central iso-line localised on a region of 15×15 mm is shown.

electron population having energy 25 MeV. This energy is similar to that of the electron beams used for radiotherapy with LINACs³⁸.

The spread of the beam pointing angle of the electron source for several consecutive shots is shown in Fig. 5(a). The electron dose distribution was measured and is shown in Fig. 5(b). After removing the magnetic spectrometer, a super-sensitive, absolutely calibrated radiochromic film (EBT3 Gafchromic) was placed 3 cm after the chamber electron exit port, normal to the electron beam propagation direction. The electron beam after passing through a 2 cm glass polymerizes the detector's material. The minimum captured energy was 6 MeV due to glass filtering⁴⁷.

The dose of 140 consecutive shots was accumulated. The accumulated dose results in a Gaussian-like distribution. It is worth noticing that at the central iso-surface region of about 10 mm in diameter, a dose ≥ 2.5 Gy is measured. The mean dose per shot is ≥ 15 mGy which exceeds the values reported in previous results from experiments conducted under similar conditions^{48,49}. When operating at 5 Hz the source it may deliver to this central area a dose of ≥ 4.5 Gy/min. This value is adequate for experiments exploring the potential use of LWFA accelerated electrons in biomedical applications³⁸.

III. TWO-DIMENSIONAL PIC SIMULATIONS

To support our experimental results and distinguish the contribution of the injection mechanisms, we performed 2D PIC simulations. The LWFA models are simulated using EPOCH PIC code⁵⁰. We used a moving window (moving at $0.995 \times c$), in the laboratory frame configuration. The computational domain size is of 120

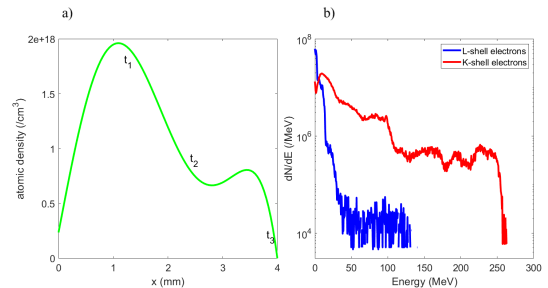


FIG. 6: (a) Polynomial approximation of atomic N density used for the PIC simulations. (b) Electron energy spectrum resulting from PIC simulations

$\times 100 \mu\text{m}$, discretized by 2048×384 cells. Two neutral N macroparticles per cell of the 5th-order particle shape function were used⁵¹. The ionization module was implemented; thus, the energy thresholds for ionization of each N electron were set respectively. Given the thresholds, in the intensity regime of this work, K-shell electrons of N are ionized only at the peak electric field of the laser pulse, while L-shell electrons are already ionized by the front lower-intensity region of the pulse (10^{16} W/cm^2). To discriminate the contribution of the co-existing injection mechanisms (downramp & ionization injection), electrons were separated into three groups, group 1 containing 5 electrons of the L-shell (already ionized before the peak electric field), and groups 2 and 3 containing 6 and 7 electrons. This approach allows for separate handling, essentially investigating the behaviour of each group. The atomic density profile has been simulated as a high-order polynomial function seen in Fig. 6(a), which approximates well the main downramp region while taking into account the first moderate density oscillation measured in Fig. 2(c), avoiding using tophat and trapezoidal approximations, thus avoiding discontinuities which are far from the measured profile and enhance injection numerically. In Fig. 6(b) the resulting spectra at the end of the simulation are presented for the sum of all K- and L-shell electrons separately. The L-shell electron population is smaller while achieving lower energy than K-shell electrons. The maximum energy approaches the maximum measured energy. Their behaviour is explained by the electron density maps seen in Fig. 7. Electron density maps of L-shell electrons (top) and K-shell (bottom) evolve at three time steps: this t_1 corresponds to the laser crossing the density peak. Fig. 7(a,d), t_2 corresponds to the end of the downramp Fig. 7(b,e) and t_3 at the end of the gas. Fig. 7(c,f). In Fig. 7(a) L-shell electrons have formed the bubble at the wake of the laser, while no electrons have yet been injected. In Fig. 7(b) the bubble has evolved to a channel after continuous elongation along the downramp, and it is evident that from the rear side of the channel a bunch of electrons is injected. This population is attributed to the downramp mechanism. Finally, in Fig. 7(c) acceler-

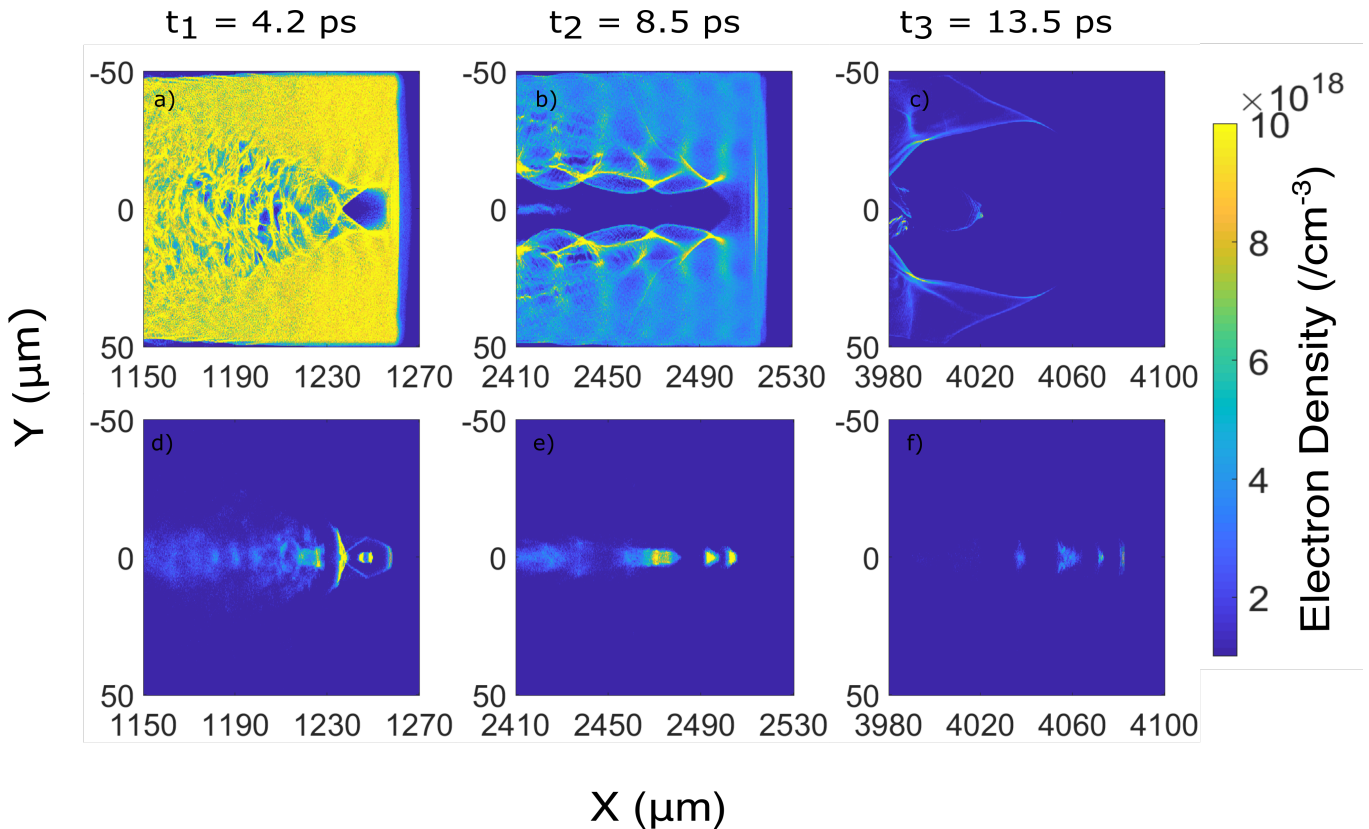


FIG. 7: PIC simulation results: time evolution of electron density for L-shell electrons (1-5) (up) and the 7th electron (K-shell) (down). Left frames correspond to the time that the laser crosses the peak of the plasma density, middle frames to the end of the downramp and right to the end of the simulations.

ated electrons are released to the free space at the end of the simulation. In Fig. 7(d,e) and (f), the presence of K-shell electrons is confirmed, especially close to the axis of propagation. Significantly fewer K-shell electrons are finally accelerated at the end of the simulation (than those ionised). Our PIC results show that the acceleration of electrons injected due to both mechanisms is confirmed. Electrons of the K-shell achieve energy up to 285 MeV. The behaviour matches well with the experimental results of accelerated electrons of 45 bars. In addition, a parametric study keeping the density profile form and varying the peak density value of the polynomial was conducted to gain more insight. By reducing density, fewer and less accelerated electrons of the L-shell are noticed in the final spectra up to the dissipation of the downramp mechanism, while in the higher density cases, downramp-injected electrons continue to accelerate efficiently. As far as K-shell electrons, their injection is confirmed for the higher- and lower-density cases. However, as the density increases, filamentation of the laser reduces the energy absorbed by the main accelerating structure and restricts their acceleration.

IV. CONCLUSIONS

In summary, we performed an experimental study, supported by numerical simulation results, of an electron source produced by laser wakefield acceleration (LWFA), using a novel-design, 3D-printed NS nozzle. The electron source characteristics, such as the electron energy, divergence, and total beam charge, were measured at different backing pressures. The results indicate a tunable high-dose, high-energy electron source. The median total charge remained almost stable as a function of the backing pressure. The electron beam divergence remained relatively high even within the optimal backing pressure. The charge/dE/shot was enhanced by at least a factor of 10 and the maximum energy by a factor of 2, compared to our previous work in which various symmetrical nozzles were implemented^{33,35,43}. The increase in the electron charge is attributed to the downramp mechanism, which reduces the injection threshold along with the ionization injection mechanism. Increasing the backing pressure resulted in the acceleration of electrons with more beam-like characteristics, with the optimal operating pressure range being in the window 45-55 bar. Nevertheless, the low-energy electron bunches generated at low backing pressures are useful for radio-

medical studies, as their energy corresponds to that of typical LINACS established in hospitals for radiotherapy (6–25 MeV)³⁸. Thus, comparative experiments can be performed to explore the potential advantages of pulsed electron sources in radiotherapy⁵². In addition, the dose profile shows a central iso-surface with significant dose accumulation. Finally, the resulting electron bunches are considered suitable for Betatron radiation emission (i.e., pump-probe experiments)^{33,53}, as this radiation is enhanced as a function of electron charge; thus, high X-ray flux is expected^{21,37,54}.

ACKNOWLEDGMENTS

The author D.M. acknowledges funding by the Hellenic Mediterranean University within the project "Proposal for post-doctoral research at the Institute of Plasma Physics and Lasers (IPPL) of Hellenic Mediterranean University (HMU)" on the context of the 2607/Φ.120/04-05-2022 call of HMU for post-doctoral research. This work was carried out within the project "Use of secondary sources of plasma radiation produced by the interaction of powerful lasers with material for biomedical applications" funded by national resources of Greece under the Regional Development Program of the Region of Crete (2024NII10200000/5220198).

The EPOCH code used in this work was in part funded by the UK EPSRC grants EP/G054950/1, EP/G056803/1, EP/G055165/1, EP/M022463/1 and EP/P02212X/1. We acknowledge the support with computational time granted by the Greek Research & Technology Network (GRNET) in the National HPC facility ARIS – under project ID pr016025-LaMPIOS III.

This work has been carried out within the framework of the EUROfusion Consortium, funded by the European Union via the Euratom Research and Training Programme (Grant Agreement No 101052200 — EUROfusion) and the Hellenic National Program of Controlled Thermonuclear Fusion. Views and opinions expressed are however those of the authors alone and do not necessarily reflect those of the European Union or the European Commission. Neither the European Union nor the European Commission can be held responsible for them.

DATA AVAILABILITY

The data that support the findings of this study are available from the corresponding author upon reasonable request.

REFERENCES

- ¹E. Adli, "Plasma wakefield linear colliders—opportunities and challenges," *Philosophical Transactions of the Royal Society A: Mathematical, Physical and Engineering Sciences* **377**, 20180419 (2019).
- ²A. J. Gonsalves, K. Nakamura, J. Daniels, C. Benedetti, C. Pieronek, T. C. H. de Raadt, S. Steinke, J. H. Bin, S. S. Bulanov, J. van Tilborg, C. G. R. Geddes, C. B. Schroeder, C. Tóth, E. Esarey, K. Swanson, L. Fan-Chiang, G. Bagdasarov, N. Bobrova, V. Gasilov, G. Korn, P. Sasorov, and W. P. Leemans, "Petawatt laser guiding and electron beam acceleration to 8 gev in a laser-heated capillary discharge waveguide," *Physical Review Letters* **122**, 084801 (2019).
- ³Y. Wu, J. Hua, Z. Zhou, J. Zhang, S. Liu, B. Peng, Y. Fang, X. Ning, Z. Nie, F. Li, C. Zhang, C.-H. Pai, Y. Du, W. Lu, W. B. Mori, and C. Joshi, "High-throughput injection–acceleration of electron bunches from a linear accelerator to a laser wakefield accelerator," *Nature Physics* **17**, 801–806 (2021).
- ⁴S. P. D. Mangles, A. G. R. Thomas, O. Lundh, F. Lindau, M. C. Kaluza, A. Persson, C.-G. Wahlström, K. Krushelnick, and Z. Najmudin, "On the stability of laser wakefield electron accelerators in the monoenergetic regime," *Physics of Plasmas* **14**, 056702 (2007).
- ⁵C. G. R. Geddes, C. Toth, J. van Tilborg, E. Esarey, C. B. Schroeder, D. Bruhwiler, C. Nieter, J. Cary, and W. P. Leemans, "High-quality electron beams from a laser wakefield accelerator using plasma-channel guiding," *Nature* **431**, 538–541 (2004).
- ⁶J. Faure, Y. Glinec, A. Pukhov, S. Kiselev, S. Gordienko, E. Lefebvre, J.-P. Rousseau, F. Burgy, and V. Malka, "A laser-plasma accelerator producing monoenergetic electron beams," *Nature* **431**, 541–544 (2004).
- ⁷S. P. Mangles, C. D. Murphy, Z. Najmudin, A. G. Thomas, J. L. Collier, A. E. Dangor, E. J. Divall, P. S. Foster, J. G. Gallacher, C. J. Hooker, and et al., "Monoenergetic beams of relativistic electrons from intense laser–plasma interactions," *Nature* **431**, 535–538 (2004).
- ⁸A. Rousse, K. T. Phuoc, R. Shah, A. Pukhov, E. Lefebvre, V. Malka, S. Kiselev, F. Burgy, J.-P. Rousseau, D. Umstadter, and D. Hulin, "Production of a kev x-ray beam from synchrotron radiation in relativistic laser-plasma interaction," *Phys. Rev. Lett.* **93**, 135005 (2004).
- ⁹A. Grigoriadis, G. Andrianaki, M. Tatarakis, E. P. Benis, and N. A. Papadogiannis, "Betatron-type laser-plasma x-ray sources generated in multi-electron gas targets," *Applied Physics Letters* **118**, 131110 (2021).
- ¹⁰J. F. Ong, A. C. Berceanu, A. Grigoriadis, G. Andrianaki, V. Dimitriou, M. Tatarakis, N. A. Papadogiannis, and E. P. Benis, "Non-linear QED approach for betatron radiation in a laser wakefield accelerator," *Scientific Reports* **14**, 605 (2024).
- ¹¹A. R. Maier, N. M. Delbos, T. Eichner, L. Hübner, S. Jalas, L. Jeppe, S. W. Jolly, M. Kirchen, V. Leroux, P. Messner, M. Schnepf, M. Trunk, P. A. Walker, C. Werle, and P. Winkler, "Decoding sources of energy variability in a laser-plasma accelerator," *Phys. Rev. X* **10**, 031039 (2020).
- ¹²D. Gustas, D. Guénot, A. Vernier, S. Dutt, F. Böhle, R. Lopez-Martens, A. Lifschitz, and J. Faure, "High-charge relativistic electron bunches from a khz laser-plasma accelerator," *Phys. Rev. Accel. Beams* **21**, 013401 (2018).
- ¹³J. P. Couperus, R. Pausch, A. Köhler, O. Zarini, J. M. Krämer, M. Garten, A. Huebl, R. Gebhardt, U. Helbig, S. Bock, K. Zeil, A. Debus, M. Bussmann, U. Schramm, and A. Irman, "Demonstration of a beam loaded nanocoulomb-class laser wakefield accelerator," *Nature Communications* **8**, 487 (2017).
- ¹⁴C. Aniculaesei, T. Ha, S. Yoffe, L. Labun, S. Milton, E. McCary, M. M. Spinks, H. J. Quevedo, O. Z. Labun, R. Sain, A. Hannasch, R. Zgadza, I. Pagano, J. A. Franco-Altamirano, M. L. Ringuette, E. Gaul, S. V. Luedtke, G. Tiwari, B. Ersfeld, E. Brunetti, H. Ruhl, T. Ditmire, S. Bruce, M. E. Donovan, M. C. Downer, D. A. Jaroszynski, and B. M. Hegelich, "The acceleration of a high-charge electron bunch to 10 gev in a 10-cm nanoparticle-assisted wakefield accelerator," *Matter and Radiation at Extremes* **9**, 014001 (2023).

¹E. Adli, "Plasma wakefield linear colliders—opportunities and challenges," *Philosophical Transactions of the Royal Society A:*

- ¹⁵D. Umstadter, S.-Y. Chen, A. Maksimchuk, G. Mourou, and R. Wagner, “Nonlinear optics in relativistic plasmas and laser wake field acceleration of electrons,” *Science* **273**, 472–475 (1996).
- ¹⁶M. Z. Mo, A. Ali, S. Fourmaux, P. Lassonde, J. C. Kieffer, and R. Fedosejevs, “Quasimonoeenergetic electron beams from laser wakefield acceleration in pure nitrogen,” *Applied Physics Letters* **100**, 074101 (2012).
- ¹⁷W. Lu, M. Tzoufras, C. Joshi, F. S. Tsung, W. B. Mori, J. Vieira, R. A. Fonseca, and L. O. Silva, “Generating multi-gev electron bunches using single stage laser wakefield acceleration in a 3d nonlinear regime,” *Physical Review ST Accelerators and Beams* **10**, 061301 (2007).
- ¹⁸C. McGuffey, A. Thomas, W. Schumaker, T. Matsuoaka, V. Chvykov, F. Dollar, G. Kalintchenko, V. Yanovsky, A. Maksimchuk, K. Krushelnick, *et al.*, “Ionization induced trapping in a laser wakefield accelerator,” *Physical review letters* **104**, 025004 (2010).
- ¹⁹M. Mirzaie, N. A. M. Hafz, S. Li, F. Liu, F. He, Y. Cheng, and J. Zhang, “Enhanced electron yield from laser-driven wakefield acceleration in high-Z gas jets,” *Review of Scientific Instruments* **86** (2015), 10.1063/1.4931780, 103502.
- ²⁰P. Tomassini, F. Massimo, L. Labate, and L. A. Gizzi, “Accurate electron beam phase-space theory for ionization-injection schemes driven by laser pulses,” *High Power Laser Science and Engineering* **10**, e15 (2022).
- ²¹D. Papp, Z. Léczy, C. Kamperidis, and N. A. M. Hafz, “Highly efficient few-cycle laser wakefield electron accelerator,” *Plasma Physics and Controlled Fusion* **63**, 065019 (2021).
- ²²F. Massimo, A. F. Lifschitz, C. Thaury, and V. Malka, “Numerical studies of density transition injection in laser wakefield acceleration,” *Plasma Physics and Controlled Fusion* **59**, 085004 (2017).
- ²³S. Maity, A. Mondal, E. Vishnyakov, and A. Molodtsov, “Parametric analysis of electron beam quality in laser wakefield acceleration based on the truncated ionization injection mechanism,” *Plasma Physics and Controlled Fusion* **66**, 035012 (2024).
- ²⁴P. Brijesh, C. Thaury, K. T. Phuoc, S. Corde, G. Lambert, V. Malka, S. P. D. Mangles, M. Bloom, and S. Kneip, “Tuning the electron energy by controlling the density perturbation position in laser plasma accelerators,” *Physics of Plasmas* **19**, 063104 (2012).
- ²⁵M. Hansson, B. Aurand, X. Davoine, H. Ekerfelt, K. Svensson, A. Persson, C.-G. Wahlström, and O. Lundh, “Down-ramp injection and independently controlled acceleration of electrons in a tailored laser wakefield accelerator,” *Phys. Rev. ST Accel. Beams* **18**, 071303 (2015).
- ²⁶L. Fan-Chiang, H.-S. Mao, H.-E. Tsai, T. Ostermayr, K. K. Swanson, S. K. Barber, S. Steinke, J. van Tilborg, C. G. R. Geddes, and W. P. Leemans, “Gas density structure of supersonic flows impinged on by thin blades for laser-plasma accelerator targets,” *Physics of Fluids* **32**, 066108 (2020).
- ²⁷K. Schmid, A. Buck, C. M. S. Sears, J. M. Mikhailova, R. Tautz, D. Herrmann, M. Geissler, F. Krausz, and L. Veisz, “Density-transition based electron injector for laser driven wakefield accelerators,” *Phys. Rev. ST Accel. Beams* **13**, 091301 (2010).
- ²⁸J. Xu, A. Buck, S.-W. Chou, K. Schmid, B. Shen, T. Tajima, M. C. Kaluza, and L. Veisz, “Dynamics of electron injection in a laser-wakefield accelerator,” *Physics of Plasmas* **24**, 083106 (2017), https://pubs.aip.org/aip/pop/article-pdf/doi/10.1063/1.4996906/15649735/083106_1_online.pdf.
- ²⁹A. Buck, J. Wenz, J. Xu, K. Khrennikov, K. Schmid, M. Heigoldt, J. M. Mikhailova, M. Geissler, B. Shen, F. Krausz, S. Karsch, and L. Veisz, “Shock-front injector for high-quality laser-plasma acceleration,” *Phys. Rev. Lett.* **110**, 185006 (2013).
- ³⁰G. Golovin, S. Chen, N. Powers, C. Liu, S. Banerjee, J. Zhang, M. Zeng, Z. Sheng, and D. Umstadter, “Tunable monoenergetic electron beams from independently controllable laser-wakefield acceleration and injection,” *Phys. Rev. ST Accel. Beams* **18**, 011301 (2015).
- ³¹V. Tomkus, V. Girdauskas, J. Dudutis, P. Gečys, V. Stankevič, G. Račiukaitis, I. Gallardo González, D. Guénot, J. B. Svensson, A. Persson, and O. Lundh, “Laser wakefield accelerated electron beams and betatron radiation from multijet gas targets,” *Scientific Reports* **10**, 16807 (2020).
- ³²Z. Lei, Z. Jin, A. Zhidkov, N. Pathak, Y. Mizuta, K. Huang, N. Nakanii, I. Daito, M. Kando, and T. Hosokai, “Controllable electron self-injection in laser wakefield acceleration with asymmetric gas-jet nozzle,” *Progress of Theoretical and Experimental Physics* **2023**, 033J01 (2023).
- ³³A. Grigoriadis, G. Andrianaki, I. Ftilis, V. Dimitriou, E. I. Clark, N. A. Papadogiannis, E. P. Benis, and M. Tatarakis, “Improving a high-power laser-based relativistic electron source: the role of laser pulse contrast and gas jet density profile,” *Plasma Physics and Controlled Fusion* **64**, 044007 (2022).
- ³⁴A. Grigoriadis, G. Andrianaki, I. Tazes, V. Dimitriou, M. Tatarakis, E. P. Benis, and N. A. Papadogiannis, “Efficient plasma electron accelerator driven by linearly chirped multi-10-tw laser pulses,” *Scientific Reports* **13** (2023), 10.1038/s41598-023-28755-1.
- ³⁵A. Grigoriadis, G. Andrianaki, M. Tatarakis, E. P. Benis, and N. A. Papadogiannis, “The role of laser chirp in relativistic electron acceleration using multi-electron gas targets,” *Plasma Physics and Controlled Fusion* **65**, 044001 (2023).
- ³⁶E. L. Clark, A. Grigoriadis, S. Petrakis, I. Tazes, G. Andrianaki, A. Skoulakis, Y. Orphanos, E. Kaselouris, I. Ftilis, J. Chatzakis, and *et al.*, “High-intensity laser-driven secondary radiation sources using the zeus 45 tw laser system at the institute of plasma physics and lasers of the hellenic mediterranean university research centre,” *High Power Laser Science and Engineering* **9**, e53 (2021).
- ³⁷J. Ferri, S. Corde, A. Döpp, A. Lifschitz, A. Doche, C. Thaury, K. Ta Phuoc, B. Mahieu, I. A. Andriyash, V. Malka, and X. Davoine, “High-brilliance betatron γ -ray source powered by laser-accelerated electrons,” *Phys. Rev. Lett.* **120**, 254802 (2018).
- ³⁸L. Labate, D. Palla, D. Panetta, F. Avella, F. Baffigi, F. Brandi, F. Di Martino, L. Fulgentini, A. Giulietti, P. Koster, D. Terzani, P. Tomassini, C. Traino, and L. A. Gizzi, “Toward an effective use of laser-driven very high energy electrons for radiotherapy: Feasibility assessment of multi-field and intensity modulation irradiation schemes,” *Scientific Reports* **10**, 17307 (2020).
- ³⁹E. L. Clark, A. Grigoriadis, S. Petrakis, I. Tazes, G. Andrianaki, A. Skoulakis, Y. Orphanos, E. Kaselouris, I. Ftilis, J. Chatzakis, and *et al.*, “High-intensity laser-driven secondary radiation sources using the zeus 45 tw laser system at the institute of plasma physics and lasers of the hellenic mediterranean university research centre,” *High Power Laser Science and Engineering* **9**, e53 (2021).
- ⁴⁰A. Grigoriadis, *Acceleration of Electrons to Relativistic Velocities Using an Ultra-Intense Laser*, Ph.D. thesis, University of Ioannina, School of Sciences, Department of Physics (2023).
- ⁴¹A. Döpp, E. Guillaume, C. Thaury, J. Gautier, K. Ta Phuoc, and V. Malka, “3d printing of gas jet nozzles for laser-plasma accelerators,” *Review of Scientific Instruments* **87**, 073505 (2016).
- ⁴²M. Vargas, W. Schumaker, Z.-H. He, Z. Zhao, K. Behm, V. Chvykov, B. Hou, A. Maksimchuk, V. Yanovsky, and A. G. R. Thomas, “Improvements to laser wakefield accelerated electron beam stability, divergence, and energy spread using three-dimensional printed two-stage gas cell targets,” *Applied Physics Letters* **104**, 174103 (2014).
- ⁴³G. Andrianaki, A. Grigoriadis, A. Skoulakis, I. Tazes, D. Mancelli, I. Ftilis, V. Dimitriou, E. P. Benis, N. A. Papadogiannis, M. Tatarakis, and I. K. Nikolos, “Design, manufacturing, evaluation, and performance of a 3d-printed, custom-made nozzle for laser wakefield acceleration experiments,” *Review of Scientific Instruments* **94**, 103309 (2023).
- ⁴⁴J. Couperus, A. Köhler, T. Wolterink, A. Jochmann, O. Zarini, H. Bastiaens, K. Boller, A. Irman, and U. Schramm, “Tomographic characterisation of gas-jet targets for laser wakefield acceleration,” *Nuclear Instruments and Methods in Physics Re-*

- search Section A: Accelerators, Spectrometers, Detectors and Associated Equipment **830**, 504–509 (2016).
- ⁴⁵M. Hipp, J. Woisetschläger, P. Reiterer, and T. Neger, “Digital evaluation of interferograms,” *Measurement* **36**, 53–66 (2004).
- ⁴⁶EPS, ed., *Proc. 48th European Physics Society (EPS) Plasma Conference* (2022).
- ⁴⁷M. Berger, J. Coursey, M. Zucker, and J. Chang, “Estar, pstar, and astar: Computer programs for calculating stopping-power and range tables for electrons, protons, and helium ions (version 1.2.3),” (2005).
- ⁴⁸E. Beyreuther, W. Enghardt, M. Kaluza, L. Karsch, L. Laschinsky, E. Lessmann, M. Nicolai, J. Pawelke, C. Richter, R. Sauerbrey, H.-P. Schlenvoigt, and M. Baumann, “Establishment of technical prerequisites for cell irradiation experiments with laser-accelerated electrons,” *Medical Physics* **37**, 1392–1400 (2010).
- ⁴⁹K. Kokurewicz, G. H. Welsh, E. Brunetti, S. M. Wiggins, M. Boyd, A. Sorensen, A. Chalmers, G. Schettino, A. Subiel, C. DesRosiers, and D. A. Jaroszynski, “Laser-plasma generated very high energy electrons (VHEEs) in radiotherapy,” in *Medical Applications of Laser-Generated Beams of Particles IV: Review of Progress and Strategies for the Future*, Vol. 10239, edited by K. W. D. Ledingham, International Society for Optics and Photonics (SPIE, 2017) p. 102390C.
- ⁵⁰T. D. Arber, K. Bennett, C. S. Brady, A. Lawrence-Douglas, M. G. Ramsay, N. J. Sircombe, P. Gillies, R. G. Evans, H. Schmitz, A. R. Bell, and C. P. Ridgers, “Contemporary particle-in-cell approach to laser-plasma modelling,” *Plasma Physics and Controlled Fusion* **57**, 113001 (2015).
- ⁵¹I. Tazes, J. F. Ong, O. Tesileanu, K. A. Tanaka, N. A. Papadogiannis, M. Tatarakis, and V. Dimitriou, “Target normal sheath acceleration and laser wakefield acceleration particle-in-cell simulations performance on cpu & gpu architectures for high-power laser systems,” *Plasma Physics and Controlled Fusion* **62**, 094005 (2020).
- ⁵²I. Ftilis, A. Grigoriadis, I. Tazes, S. Petrakis, G. Andrianaki, V. Dimitriou, E. Bakarezos, E. P. Benis, I. Tsiapa, T. Boursianis, G. Kalaitzakis, G. Bontzos, D. A. Liakopoulos, E. Pappas, E. T. Detorakis, E. L. Clark, T. G. Maris, N. A. Papadogiannis, and M. Tatarakis, “Polymer-gel radiation dosimetry of laser-based relativistic electron sources for biomedical applications: First qualitative results and experimental challenges,” *Frontiers in Physics* **10** (2022), 10.3389/fphy.2022.727511.
- ⁵³K. Huang, D. Z. Li, W. C. Yan, M. H. Li, M. Z. Tao, Z. Y. Chen, X. L. Ge, F. Liu, Y. Ma, J. R. Zhao, N. M. Hafz, J. Zhang, and L. M. Chen, “Simultaneous generation of quasi-monoenergetic electron and betatron X-rays from nitrogen gas via ionization injection,” *Applied Physics Letters* **105**, 204101 (2014).
- ⁵⁴C. Emma, J. Van Tilborg, R. Assmann, S. Barber, A. Cianchi, S. Corde, M. E. Couprie, R. D’Arcy, M. Ferrario, A. F. Habib, and et al., “Free electron lasers driven by plasma accelerators: status and near-term prospects,” *High Power Laser Science and Engineering* **9**, e57 (2021).